Protective role of the nucleic acid sensor STING in pulmonary fibrosis Running title: STING protects against IPF

Florence Savigny, Corinne Schricke, Norinne Lacerda-Queiroz, Mélanie Meda, Mégane Nascimento, Sarah Huot-Marchand, Felipe da Gama Monteiro, Bernhard Ryffel, Aurélie Gombault, M Le Bert, et al.

Protective role of the nucleic acid sensor STING in pulmonary fibrosis

Running title: STING protects against IPF

Florence Savigny[1], Corinne Schricke[1], Norinne Lacerda-Queiroz[1], Mélanie Meda[1], Mégane Nascimento[1], Sarah Huot-Marchand[1], Felipe Da Gama Monteiro[1], Bernhard Ryffel[1], Aurélie Gombault[1], Marc Le Bert[1], Isabelle Couillin[1] and Nicolas Riteau[1]

[1]*Experimental and Molecular Immunology and Neurogenetics laboratory, CNRS, UMR7355 and University of Orleans, France.*

Address of correspondence to Nicolas Riteau and Isabelle Couillin, E-mail : nicolas.riteau@cnrs-orleans.fr, couillin@cnrs-orleans.fr INEM, UMR 7355, 3B, rue de la Férollerie, 45071 Orleans, France.

Phone: 0033 238 25 54 43 Fax: 0033 238 25 79 79.

Keywords: idiopathic pulmonary fibrosis, STING, self-DNA recognition, mice, IL-28

Abstract

Idiopathic pulmonary fibrosis (IPF) is the most common and severe type of interstitial lung disease for which current treatments display limited efficacy. IPF is largely driven by host-derived danger signals released upon recurrent local tissue damage. Here we explored the roles of self-DNA and stimulator of interferon genes (STING), a protein belonging to an intracellular DNA sensing pathway that leads to type I and/or type III interferon (IFN) production upon activation. Using a mouse model of IPF, we report that STING deficiency leads to exacerbated pulmonary fibrosis with increased collagen deposition in the lungs and excessive remodeling factors expression. We further show that STING-mediated protection does not rely on type I IFN signaling nor on IL-17A or TGF-β modulation but is associated with dysregulated neutrophils. Together, our data support an unprecedented immunoregulatory function of STING in lung fibrosis.

Introduction

Idiopathic pulmonary fibrosis (IPF) is the most common type of idiopathic interstitial pneumonia (1, 2), characterized by progressive lung scarring causing shorter life expectancy and high mortality rate (2, 3). While the etiology is still unclear, it is believed that the physiopathology relies on repeated local micro-injuries triggering DNA damage, unbalanced cell death and aberrant tissue remodeling with extracellular matrix components and ultimately fibrosis (1-4). Immune cells such as macrophages, neutrophils and T helper 17 (Th17) cells recruited to the lung tissue are known to display important proinflammatory and profibrotic functions (5). Self-derived danger-associated molecular patterns (DAMPS) are considered as important contributors (6), such as ATP (7) and uric acid (8) to the pathology. In this study, we hypothesize that self-nucleic acid sensing might

also contribute to IPF. Pathogen-derived nucleic acid sensing through pathogen recognition receptors (PRRs) is an effective strategy to detect invading microorganisms and trigger innate and adaptive immune responses (9). However, recent literature clearly established that PRRs such as STING are also involved in self-nucleic acid sensing (10, 11). STING is an endoplasmic reticulum (ER)-associated membrane protein activated by cyclic dinucleotides (CDNs) produced as second messengers by microorganisms or synthesized by enzymes such as cyclic GMP-AMP synthase (cGAS) in response to binding either host- or pathogen-derived cytosolic dsDNA (12, 13). Of note, In addition to cGAS other cytosolic receptors such as DDX41 and IFI16 sense DNA or CDNs to activate STING (12, 13). Activated STING translocates from the ER membrane to the Golgi apparatus, induces nuclear factor κB (NF-κB) and interferon regulatory factor 3 (IRF3) transcription factors activation leading to the production of type I IFNs and other cytokines involved in host immune responses (14). Recent studies showed that STING stimulation can also lead to type III interferon production (15-17). The type III IFN family comprises IFN-λ1 (IL-29), IFN-λ2 (IL-28A), IFN-λ3 (IL-28B) and the newly identified IFN-λ4 in human and IFN-λ2 (IL-28A) and IFN-λ3 (IL-28B) in mice (18). Type III IFN are less well characterized and are thought to function similarly as type I IFN, although in a more restricted manner as their effects are most evident on epithelial cells and neutrophils (18, 19).

Detection of aberrant self-nucleic acids in the cytosol, either mitochondrial DNA (mtDNA) or nuclear DNA (14, 20), is implicated in the development of autoimmune diseases and sterile inflammation (21). Since IPF physiopathology involves unbalanced cell death processes, we investigated whether self-nucleic acid release and its sensing by the STING pathway are participating in the response (1-4). We employed the classical murine model of human IPF using airway exposure to bleomycin (BLM), a potent cytotoxic drug used as chemotherapy but causing

pulmonary fibrosis in a fraction of treated patients (22). We show that intranasal BLM administration leads to increased levels of self-DNA in the airways and upregulated cGAS and STING expressions. We report that STING deficiency leads to an exacerbated lung fibrosis independently of type I IFN signaling and characterized by a prolonged neutrophilic inflammation. As a whole, our data show that STING is protective against BLM-induced pulmonary fibrosis in a mechanism that may rely on neutrophilic inflammation resolution.

Material and methods

Mice

Wild-type C57BL/6J (WT) mice were purchased from Janvier laboratory (Janvier Laboratory, France). Mice deficient for STING (*Sting*$^{-/-}$) were provided by Glen Barber (23), *Cgas*$^{-/-}$ by Zhijian Chen (24) and *Ifnar1*$^{-/-}$ by Michel Aguet (25) and bred in our specific pathogen-free animal facility at CNRS (TAAM UPS44, Orleans, France). For experiments, adult (8–14-week-old) males were transferred to experimental animal facility and monitored daily.

Ethics

All animal experiments complied with the French Government animal experiment regulations and were submitted to the "Ethics Committee for Animal Experimentation of CNRS Campus Orleans" (CCO) under number CLE CCO 2015-1087 and approved under APAFIS#19361. Clinical score was determined daily based on mice appearance and behavior. Appearance was determined based on standard parameters including eye, fur and ear monitoring

(https://www.nc3rs.org.uk/grimacescales) and behavior monitoring included mobility, posture and social interaction.

Treatments

Bleomycin sulfate (7.5 mg/kg and 3 mg/kg for day 1 and day 14 experiments, respectively; Bellon Laboratories) in saline or saline alone were administered through the airways by nasal instillation in a volume of 40µl under light isoflurane anesthesia.

Bronchoalveolar lavage and cell counts

Mice were euthanized by CO_2 overdose using Prodigy Lab Control Unit (Smartbox) and bronchoalveolar lavage fluid (BALF) was performed as previously described (7). Differential cell counts were routinely controlled on cytospin preparation (Cytospin 3, Thermo Shandon) after May-Grünwald Giemsa staining (Sigma Aldrich, St Louis, MO) according to the manufacturer's instructions and at least 200 cells were counted using standard morphological criteria.

Lung homogenization

After BALF collection, lungs were perfused with isoton to flush the vascular content and homogenized by a rotor-stator (Ultra-turrax®) in 1 ml of PBS. The extracts were centrifuged for 10 min at 9,000 g and supernatants stored at -80°C.

Lung histology

Lung left lobes were fixed in 4% buffered formaldehyde, processed and paraffin-embedded under standard conditions. Lung sections (3 µm) were stained with haematoxylin and eosin (H&E) or

Sirus red/Fast green. The slides were scanned using NanoZoomer (Hamamatsu Photonics France) and lung fibrosis scored using the Ashcroft modified scale (26).

Mediator measurement

BALF supernatants and lung homogenates were analyzed using ELISA assay kits for murine CXCL1/KC, MMP-9 and TIMP-1 according to manufacturer's instructions (R&D system, Minneapolis, MN). TGFβ1-3 contents in the lungs were assessed by multiplex assay according to manufacturer's instructions (Merck, Darmstadt, Germany).

Collagen assay

BALF collagen content was measured using the Sircol collagen dye binding assay (Biocolor Ltd., Northern Ireland) according to the manufacturer's instructions.

Double-stranded (ds)DNA quantification

Cell-free dsDNA was measured in the BALF fluid using Quant-iTPicoGreen dsDNA reagent (Invitrogen, Carlsbad, CA), according to the manufacturer's protocol.

Quantitative PCR

RNA was purified from lung homogenates using Tri-Reagent (Sigma-Aldrich, Saint-Louis, MO) extraction protocol. RNA reverse transcription into cDNA was carried out with GoTaq qPCR-Master Mix (Promega, Madison, WI). RT-qPCR was performed with Fast SYBR Green Master mix (Promega) on an ARIA MX (Agilent Technologies, Santa Clara, CA). Primers *Tmem173* (#QT00261590) encoding for STING, *Mb21d1* (#QT00131929) encoding for cGAS and *Fn1* (#QT00135758) encoding for fibronectin were purchased from Qiagen (Qiagen, Hilden,

Germany). RNA expression was normalized to *Gapdh* (#QT00166768, Qiagen, Hilden, Germany) expression and analyzed using the ΔΔCt method.

Flow cytometry

Lungs were cut in small pieces and digested using a 1mg/ml DNase (DN25, Sigma Aldrich, St Louis, MO) / 125µg/ml collagenase (Liberase^{TM}, Sigma Aldrich, St Louis, MO) solution for 45 min at 37°C and filtered on 40µm cell strainer. BALF and lung single cell suspensions were incubated for 20 min at RT with Fc block (ThermoFisher Scientific, Waltham, MA), washed and stained with surface markers including a Fixable Viability Dye eFluor 780 (ThermoFisher Scientific, Waltham, MA). Cells were fixed and permeabilized using Fixation/Permeabilization kit (ThermoFisher Scientific, Waltham, MA) and stained with intracellular markers. For IL-17 staining (clone eBio17B7), lung cell suspensions were incubated for 5 hours at 37°C in presence of brefeldin A (BFA; ThermoFisher Scientific, Waltham, MA) to prevent protein secretion. Antibody clones and dilutions used are detailed in supplementary Table 1. All samples were acquired on an LSR Fortessa flow cytometer (BD Biosciences, San Jose, CA) and analyzed using FlowJo software (TreeStar).

Immunoblot

20µg of proteins (Pierce BCA protein assay, ThermoFisher Scientific, Waltham, MA) were denatured by boiling (95 °C, 5 min) in reducing SDS sample buffer, separated by SDS-PAGE and transferred to nitrocellulose membranes (GE Healthcare Life Sciences, Amersham, UK). After blocking in 5% Blotting-Grade Blocker (BioRad, France) and washing in Tris-Buffered saline (TBS)- 0,1% Tween® 20, membranes were incubated with primary mouse anti-STING (Abcam, ref ab92605), anti-cGAS (Cell Signaling Technology, ref 3165) or anti-IL28 (Santa Cruz

Biotechnology, ref sc-137151) antibodies in TBS-BSA (Bovine Serum Albumine) 1%- azide 0,5 mM overnight at 4°C. Membranes were washed and incubated with relevant secondary antibody conjugated to horseradish peroxidase (HRP) two hours at RT. Anti-actin antibody was already HRP-conjugated (Sigma Aldrich, ref A3854). Detection was performed with ECL Western-blotting Detection Reagent (GE Healthcare Life Sciences, Amersham, UK) and luminescence acquired using Multi-application gel imaging system PXi software (Syngene). Bands intensity were quantified using ImageJ (NIH, USA).

Immunofluorescence

Lung tissues were fixed in 4% paraformaldehyde (PFA) (Sigma Aldrich, St Louis, MO) and then dehydrated in 30% sucrose solution for two weeks at 4°C. Lungs were embedded in tissue-teck (OCT®), and stored at -80°C. 10µm lung sections were cut on cryostat (Leica, Solms, Germany) and heated at 80° C for 30 min in 10mM citrate pH = 6. Lung cells were permeabilized with 0.5% Triton X-100, blocked in 1% BSA 10% SVF 0.1% Triton X-100 in PBS for 1h, washed three times in TBS and incubated overnight with rabbit anti-STING (ab92605 1/50, Abcam) in PBS containing 2% BSA, 10% FCS and 0.5% Triton X-100 at 4°C. Lung sections were TBS washed and incubated with anti-rabbit IgG Alexa 532 secondary antibody (1/100) for 1h at RT. After washing, cells were counterstained with DAPI for 10 min at RT, PBS washed and mounted onto microscope slides (mowiol). Slides were observed using a Zeiss Axiovert 200M microscope coupled with a Zeiss LSM 510 Meta scanning device (Carl Zeiss Co. Ltd., Jena, Germany). The inverted microscope was equipped with a Plan-Apochromat 63X objective (NA = 1.4) Images were acquired using Zeiss LSM Image Browser (Carl Zeiss Co. Ltd., Jena, Germany).

Statistical analyses

Statistical tests of selected populations were performed using Mann-Whitney non-parametric test. Body weight variation plots were analyzed using Two-Way Anova corrected for multiple comparisons employing Tuckey's test. Results were considered significant at $p < 0.05$.

Results

BLM administration induces airway self-DNA release and lung cGAS and STING expressions

To address a potential role for self-DNA recognition by the cGAS/STING pathway in the establishment of pulmonary fibrosis, we measured double stranded (ds) DNA content in the bronchoalveolar lavage fluid (BALF) as well as cGAS and STING expressions in the lungs at the fibrotic phase (14 days after BLM instillation). As compared to saline (NaCl) control wild-type (WT) mice, we noted that dsDNA content is significantly increased in the BALF of BLM-treated WT mice (**Fig. 1A**) and BLM treatment leads to a strong increase of cGAS (*Mb21D1*) (**Fig. 1B**) and STING (*Tmem173*) (**Fig. 1C**) gene expressions in the lungs. Of note, *Mb21D1* and *Tmem173* expressions are reduced in absence of STING and cGAS, respectively, suggesting retroactive loops at the gene expression level. We next assessed cGAS and STING protein expressions in saline- or BLM-treated WT mice, cGAS ($Cgas^{-/-}$) or STING ($Sting^{-/-}$) deficient mice. Both cGAS and STING protein expressions are increased in the lungs of BLM-treated WT mice and cGAS or STING levels are not impaired by the absence of STING or cGAS, respectively (**Fig. 1D**-**E**). We also

assessed STING expression in pulmonary tissue by immunofluorescence and show that it is expressed in both bronchial epithelial cells and infiltrating cells (**Fig. 1F and 1G**).

Regarding the acute inflammatory phase (1 day after BLM instillation), we observed that despite a strong increase of BALF dsDNA content (**Suppl. Fig. 1A**), cGAS or STING deficiency had no major impact on total BALF cell numbers (**Suppl. Fig. 1B**) or neutrophil frequencies (**Suppl. Fig. 1C**). Lung levels of the neutrophil attractant chemokine CXCL1 as well as the remodeling factors MMP-9 and TIMP-1 (**Suppl. Fig. 1D-F**) were also unchanged among BLM-treated groups suggesting minor cGAS/STING contribution in early inflammation. Nevertheless, persistent enhanced airway dsDNA in the BALF associated with a strong increase of lung cGAS and STING expressions at the fibrotic stage led us to investigate a role for this pathway in the establishment of pulmonary fibrosis.

STING deficiency leads to increased pulmonary fibrosis

As compared to BLM-treated WT or *Cgas*$^{-/-}$ mice, *Sting*$^{-/-}$ mice exhibit higher body weight loss (**Fig. 2A**) with occasional succumbing animals. The remodeling factors MMP-9 (**Fig. 2B**) and TIMP-1 (**Fig. 2C**) were also increased in the lungs of STING deficient animals as compared to their WT relatives 14 days post BLM administration. This was accompanied by higher lung cell accumulation as shown by H&E staining of lung micrographs (**Fig. 2D**) and $CD4^+$ T lymphocyte numbers assessed by flow cytometry (**Fig. 2E**). Sirius Red/Fast Green collagen staining also shows extended areas of fibrosis and increased collagen deposition (**Fig. 2F**), further confirmed by fibrosis score using Ashcroft modified scale (26) (**Fig. 2G**). BALF collagen content was also increased in *Sting*$^{-/-}$ mice as compared to their WT relatives (**Fig. 2H**). Interestingly, BLM-treated *Cgas*$^{-/-}$ mice display intermediate bodyweight loss (**Fig. 2A**), MMP-9 production (**Fig. 2B**) and

fibrosis (**Fig. 2F-G**), suggesting that other DNA sensors might be involved. Of note, BLM-induced increased levels of the important pro-fibrotic factor TGF-β were not significantly altered in cGAS or STING deficient mice **(Fig. 2I)**, arguing for a role of another pro-fibrotic pathway in absence of STING.

STING-mediated protection is type I IFN signaling independent

STING signaling pathway is a well-characterized type I IFN inducer (14). We thus utilized mouse deficient for type I IFN receptor (*Ifnar1*$^{-/-}$) to test the hypothesis of a type I IFN-dependent role of STING. In contrast to BLM-treated *Sting*$^{-/-}$ mice, *Ifnar1*$^{-/-}$ displayed comparable body weight loss as WT mice (**Fig. 3A**). In addition, lung remodeling factors MMP-9 and TIMP-1 were similarly increased comparing BLM-treated WT versus *Ifnar1*$^{-/-}$ mice, while *Sting*$^{-/-}$ mice displayed higher expressions (**Fig. 3B-C**). *Ifnar1*$^{-/-}$ mice did not display enhanced lung cell influx (**Fig. 3D**) and lung fibrosis as shown by representative lung histology (**Fig. 3E**) and Ascroft fibrosis score (**Fig. 3F**) as well as the expression of the extracellular matrix protein fibronectin (*Fn1*) (**Fig. 3G**). Together, these results suggest that STING is protective against BLM-induced fibrosis in a type I IFN-independent manner. Since IL-17A is a major pro-fibrotic cytokine (27) and in line with a recent study showing that STING-mediated protection relies of IL-17A modulation (28), we analyzed IL-17A production by CD4^{+} T lymphocytes using flow cytometry (**Suppl. Fig. 2A-B**). We show no difference in terms of frequencies (**Fig. 3H**) or total numbers (**Fig. 3I**) of IL-17^{+} CD4^{+} T cells comparing WT and *Sting*$^{-/-}$ mice. Unexpectedly, *Ifnar1*$^{-/-}$ CD4^{+} T lymphocytes displayed lower frequency of IL-17+ cells in the lungs. Having excluded a major role for type I IFN and IL-17A to explain STING-dependent protection, we next investigated a potential role for IL-28 (type

III IFN) (15-17). Interestingly, we show that BLM induces IL-28 in the lungs and that its production partially depends on STING (**Suppl. Fig. 3A-C**).

STING deficiency affects neutrophil numbers and function

The fibrotic stage of the pathology is accompanied by the recruitment of adaptive immune cells. As expected, at this time point the main BALF cell populations in WT mice are $CD4^+$ and $CD8^+$ T lymphocytes as well as B lymphocytes, and the proportion of neutrophils is low (**Fig. 4A-B**). In contrast, neutrophils remained high in BALF and lungs of STING deficient mice (**Fig. 4B-E and Suppl. Fig. 4A-B**). We performed kinetic studies and found that BALF neutrophils persisted by day 8-14 post BLM treatment (**Fig. 4F**), suggesting prolonged inflammation. In addition to increased numbers in the BALF, lung STING deficient neutrophils (**Suppl. Fig. 4B**) display reduced MHC-II upregulation following BLM treatment as compared to their WT counterparts (**Fig. 4G and 4H**). In contrast, STING-deficient neutrophils show a strong upregulation of Arginase-1 expression (**Fig. 4I and 4J**), suggesting that STING controls neutrophil persistence and function.

Discussion

STING has been identified in 2008 as an endoplasmic reticulum receptor that induces innate immune responses (29) and is currently a hot topic in several fields including cancer immunotherapy (30), vaccines (31) and autoimmunity (32, 33). Depending on the

249 microenvironment and responsive cell types, enhancing STING signaling pathway might favor
250 antitumor activity for instance by promoting IFN-β-dependent T cell priming (34). On the other
251 hand, constitutive self-DNA-mediated sustained STING activation induces tolerance breakdown
252 and autoimmunity (32, 33).

253 There are several STING allelic variants in the general population (35) and STING-associated
254 vasculopathy with onset in infancy (SAVI) is an autoinflammatory disease caused by gain-of-
255 function mutations in *TMEM173* (36, 37). Affected children display constitutive STING activation
256 leading to increased *IFNB1* transcription and even higher transcripts levels upon cGAMP
257 stimulation, whereas other pro-inflammatory gene levels such as interleukin-1 (*IL1*), interleukin-
258 6 (*IL6*) and tumor necrosis factor (*TNF*) remain unaffected (36). In addition to cutaneous
259 vasculopathy, a major feature of SAVI is interstitial lung disease (38). Of note, the STING knock-
260 in mouse strain (V154M) corresponding to a recurrent mutation in SAVI patients exhibit a severe
261 combined immunodeficiency disease (SCID) phenotype (39).

262 Here, we employed the classical murine model of idiopathic pulmonary fibrosis (IPF) induced by
263 BLM administration in the airways. We show that BLM induces a strong increase of cell-free self-
264 DNA in the airways, which can act as a danger signal by triggering DNA sensing pathways to
265 activate innate immune responses (40) and notably in the lungs (11). However, the mechanisms by
266 which self-DNA becomes accessible for intracellular DNA sensors remain uncertain. Several
267 context-dependent pathways have been reported, such as IgG- or HMGB1-bound DNA
268 internalization following interaction with FcγRIIa or receptor for advanced glycation end products
269 (RAGE), respectively (41). The antimicrobial peptide LL37 was shown to transport extracellular
270 DNA into the cytoplasm of human primary monocytes triggering STING activation (42). IL-10-
271 family member IL-26 binds to genomic, mtDNA or neutrophil extracellular traps (NETS) DNA

and traffic them into the cytosol of human myeloid cells activating STING (43). Further investigations are required to decipher the respective contributions of nuclear DNA versus mtDNA in activating the STING pathway. Elevated plasma mtDNA copy numbers in IPF patients predicts death (44), however it remains unsure whether mtDNA is a mere marker or whether it actually modulates pathology.

Investigating sensors involved in self-DNA recognition, our results indicate that the cGAS/STING pathway does not seem to play a major role in the early airway inflammatory response, as we did not observe major changes in terms of canonical markers such as neutrophil recruitment and remodeling factors production comparing WT versus cGAS or STING deficient mice. In contrast, our data show that STING-dependent responses are important during the fibrotic stage of the disease. First, lung cGAS and STING expressions are increased both at gene and protein levels. Interestingly, Mb21D1 (encoding for cGAS) gene expression but not cGAS protein is decreased in STING deficient animals suggesting potential cross regulation. In addition, STING deficiency leads to increased lung fibrosis, as characterized by higher histological score, collagen deposition and remodeling factors expression. A protective role of STING in IPF patients has been reported recently. Authors show that blood mononuclear cells from patients undergoing acute exacerbation display significantly reduced STING protein levels correlating with decreased partial oxygen pressure (45). In addition, patients showing clinical improvement post-treatment had higher STING protein levels as compared to patients with worsen condition (45). STING has also been shown to elicit protective responses in experimental autoimmune encephalitis by dampening effector T cell infiltration and inducing dominant T cell regulatory response (46). On the other hand, STING contributes to pathology in a number of other disease settings, including silica-induced lung inflammation (47) and carbon-tetrachloride (CCl4)-induced liver fibrosis (48). These

discrepancies might reflect fine-tuning of STING signaling as well as potential differences in the kinetics and cell subsets involved.

We sought to determine STING-dependent signaling pathway mediating protection in the context of lung fibrosis and first addressed the role of type I IFN. Interestingly, our results show that STING-dependent effect does not rely on type I IFN signaling as mice deficient for its receptor do not display exacerbated pathology. While type I IFN induction is a major consequence of STING activation, several publications demonstrated that this cytokine does not directly contribute to STING-dependent effect in a number of situations. For instance, STING-associated lung disease due to a gain of function mutation in the protein (N153S) is T cell dependent but does not require IRF3/IRF7 or IFNAR (49). Similarly, SCID phenotype in STING V154M mice occurs similarly when type I IFN signaling is absent (39). STING-associated vasculopathy also develops independently of IRF3 in mice (50). Besides type I IFN induction, several publications showed STING-dependent type III IFN induction (IL-28/IL-29) in the context of viral infection (16) as well as exogenous DNA (17) or di-GMP mucosal adjuvant (15) stimulations. Interestingly, a SAVI patient presented increased plasma IL-29 expression (51). Here, we show that BLM triggers IL-28 and that its production is decreased in STING deficient mice as compared to their WT relatives. Type III IFN was shown to suppress neutrophil response either by directly limiting its influx in a collagen-induced arthritis model (52) or by primarily modifying neutrophil effector functions via posttranslational modifications in the gut (53). Follow-up experiments are needed to delineate the exact contribution of type III interferons in experimental lung fibrosis. Another possibility to explain a protective role of STING was its potential action on IL-17A production, a potent pro-fibrotic cytokine (27). Indeed, STING deficiency was reported to enhance Th17 polarization and IL-17A production therefore promoted pancreatic inflammation and fibrosis (28). However, in our

model IL-17A production by $CD4^+$ T cells was not increased in STING deficient mice as compared to their WT relatives. In our experimental setup, we found that while mice deficient for type I IFN signaling did not show altered fibrosis, their lung $CD4^+$ T lymphocytes display lower frequencies of IL-$17A^+$ cells. In addition, our data indicate that cGAS deficiency does not fully mirror STING deficiency phenotype, as BLM-treated *Cgas*$^{-/-}$ mice displayed increased expression of the fibrosis-associated remodeling factors MMP-9 and TIMP-1 as compared to WT animals but intermediate weight loss and similar Ashcroft histological score. These results suggest an intricate role of cGAS in the development of experimental lung fibrosis and that other DNA sensors might be involved such as DDX41 or IFI16 (13, 54, 55). Interestingly, it was recently shown that etoposide-induced DNA damage leads to cGAS-independent STING activation (56) while on the other hand cGAS protects hepatocytes by triggering autophagy independently of STING in mouse models of ischemia-reperfusion (57).

We report that STING deficiency leads to sustained BALF and lung neutrophil infiltration following BLM administration. Additional experiments are required to determine whether prolonged BALF and lungs neutrophil presence in the context of STING deficiency reflects different tissue lifespan and/or recurrent neutrophils recruitment. Airway neutrophilia has been associated with early mortality in IPF (58) and concentrations of the neutrophil chemoattractant CXCL8 are increased in IPF patients (59). Interestingly, we show that lung neutrophils from STING deficient mice exhibit higher levels of arginase-1. L-arginine catabolism by iNOS and arginase is related to cytotoxicity and tissue repair and classically associated with pro- versus anti-inflammatory functions of macrophages, respectively (60, 61). Interestingly, L-arginine levels in the lungs of BLM-treated mice decrease due to increased arginase-1 expression and the addition of an arginase inhibitor limits TGF-β-induced collagen production by fibroblasts (62 473). It

remains to be investigated whether neutrophil-derived arginase-1 can influence fibroblast function. In addition, we also report lower MHC II levels on STING-deficient lung neutrophils. Neutrophil are able to perform MHC-II-mediated antigen presentation to $CD4^+$ T cells (63) and recent literature reviewed the regulatory roles of neutrophils in adaptive immunity (64). However, the exact meaning of reduced MHC-II expression on STING-deficient neutrophils following BLM treatment is unclear, potentially reflecting altered T cell activation properties. As a whole, our data show an unexpected regulatory function of STING to limit BLM-induced pulmonary fibrosis associated with neutrophilic inflammation regulation.

Funding

This work was supported by Centre National de la Recherche Scientifique (CNRS), the University of Orléans, The Region Centre Val de Loire (2003-00085470), the «Conseil Général du Loiret» and the European Regional Development Fund (FEDER N° 2016-00110366 and EX005756).

Acknowledgments

The authors thank Nathalie Froux, Mathilde Fravat and all technicians from our specific pathogen-free animal facility at CNRS (TAAM UPS44, Orleans, France) for breeding and animal care. We thank Valérie Quesniaux for support and helpful discussions.

References

1. King, T. E., Jr., A. Pardo, and M. Selman. 2011. Idiopathic pulmonary fibrosis. *Lancet* 378: 1949-1961.
2. Richeldi, L., H. R. Collard, and M. G. Jones. 2017. Idiopathic pulmonary fibrosis. *Lancet* 389: 1941-1952.
3. Martinez, F. J., H. R. Collard, A. Pardo, G. Raghu, L. Richeldi, M. Selman, J. J. Swigris, H. Taniguchi, and A. U. Wells. 2017. Idiopathic pulmonary fibrosis. *Nat Rev Dis Primers* 3: 17074.
4. Strieter, R. M., and B. Mehrad. 2009. New mechanisms of pulmonary fibrosis. *Chest* 136: 1364-1370.
5. Wynn, T. A., and T. R. Ramalingam. 2012. Mechanisms of fibrosis: therapeutic translation for fibrotic disease. *Nat Med* 18: 1028-1040.
6. Ellson, C. D., R. Dunmore, C. M. Hogaboam, M. A. Sleeman, and L. A. Murray. 2014. Danger-associated molecular patterns and danger signals in idiopathic pulmonary fibrosis. *Am J Respir Cell Mol Biol* 51: 163-168.
7. Riteau, N., P. Gasse, L. Fauconnier, A. Gombault, M. Couegnat, L. Fick, J. Kanellopoulos, V. F. Quesniaux, S. Marchand-Adam, B. Crestani, B. Ryffel, and I. Couillin. 2010. Extracellular ATP is a danger signal activating P2X7 receptor in lung inflammation and fibrosis. *American journal of respiratory and critical care medicine* 182: 774-783.
8. Gasse, P., N. Riteau, S. Charron, S. Girre, L. Fick, V. Petrilli, J. Tschopp, V. Lagente, V. F. Quesniaux, B. Ryffel, and I. Couillin. 2009. Uric acid is a danger signal activating NALP3 inflammasome in lung injury inflammation and fibrosis. *American journal of respiratory and critical care medicine* 179: 903-913.
9. Akira, S., S. Uematsu, and O. Takeuchi. 2006. Pathogen recognition and innate immunity. *Cell* 124: 783-801.
10. Ahn, J., and G. N. Barber. 2014. Self-DNA, STING-dependent signaling and the origins of autoinflammatory disease. *Current opinion in immunology* 31: 121-126.
11. Benmerzoug, S., B. Ryffel, D. Togbe, and V. F. J. Quesniaux. 2019. Self-DNA Sensing in Lung Inflammatory Diseases. *Trends in immunology* 40: 719-734.
12. Jonsson, K. L., A. Laustsen, C. Krapp, K. A. Skipper, K. Thavachelvam, D. Hotter, J. H. Egedal, M. Kjolby, P. Mohammadi, T. Prabakaran, L. K. Sorensen, C. Sun, S. B. Jensen, C. K. Holm, R. J. Lebbink, M. Johannsen, M. Nyegaard, J. G. Mikkelsen, F. Kirchhoff, S. R. Paludan, and M. R. Jakobsen. 2017. IFI16 is required for DNA sensing in human macrophages by promoting production and function of cGAMP. *Nat Commun* 8: 14391.
13. Parvatiyar, K., Z. Zhang, R. M. Teles, S. Ouyang, Y. Jiang, S. S. Iyer, S. A. Zaver, M. Schenk, S. Zeng, W. Zhong, Z. J. Liu, R. L. Modlin, Y. J. Liu, and G. Cheng. 2012. The helicase DDX41 recognizes the bacterial secondary messengers cyclic di-GMP and cyclic di-AMP to activate a type I interferon immune response. *Nat Immunol* 13: 1155-1161.
14. Barber, G. N. 2015. STING: infection, inflammation and cancer. *Nat Rev Immunol* 15: 760-770.
15. Blaauboer, S. M., S. Mansouri, H. R. Tucker, H. L. Wang, V. D. Gabrielle, and L. Jin. 2015. The mucosal adjuvant cyclic di-GMP enhances antigen uptake and selectively activates pinocytosis-efficient cells in vivo. *Elife* 4.
16. Kim, J. A., S. K. Park, S. W. Seo, C. H. Lee, and O. S. Shin. 2017. STING Is Involved in Antiviral Immune Response against VZV Infection via the Induction of Type I and III IFN Pathways. *J Invest Dermatol* 137: 2101-2109.
17. Sui, H., M. Zhou, H. Imamichi, X. Jiao, B. T. Sherman, H. C. Lane, and T. Imamichi. 2017. STING is an essential mediator of the Ku70-mediated production of IFN-lambda1 in response to exogenous DNA. *Sci Signal* 10.

18. Lazear, H. M., T. J. Nice, and M. S. Diamond. 2015. Interferon-lambda: Immune Functions at Barrier Surfaces and Beyond. *Immunity* 43: 15-28.
19. Zanoni, I., F. Granucci, and A. Broggi. 2017. Interferon (IFN)-lambda Takes the Helm: Immunomodulatory Roles of Type III IFNs. *Front Immunol* 8: 1661.
20. West, A. P., and G. S. Shadel. 2017. Mitochondrial DNA in innate immune responses and inflammatory pathology. *Nat Rev Immunol* 17: 363-375.
21. Ablasser, A., C. Hertrich, R. Wassermann, and V. Hornung. 2013. Nucleic acid driven sterile inflammation. *Clin Immunol* 147: 207-215.
22. Liu, T., F. G. De Los Santos, and S. H. Phan. 2017. The Bleomycin Model of Pulmonary Fibrosis. *Methods Mol Biol* 1627: 27-42.
23. Ahn, J., D. Gutman, S. Saijo, and G. N. Barber. 2012. STING manifests self DNA-dependent inflammatory disease. *Proceedings of the National Academy of Sciences of the United States of America* 109: 19386-19391.
24. Li, X. D., J. Wu, D. Gao, H. Wang, L. Sun, and Z. J. Chen. 2013. Pivotal roles of cGAS-cGAMP signaling in antiviral defense and immune adjuvant effects. *Science* 341: 1390-1394.
25. Muller, U., U. Steinhoff, L. F. Reis, S. Hemmi, J. Pavlovic, R. M. Zinkernagel, and M. Aguet. 1994. Functional role of type I and type II interferons in antiviral defense. *Science* 264: 1918-1921.
26. Hubner, R. H., W. Gitter, N. E. El Mokhtari, M. Mathiak, M. Both, H. Bolte, S. Freitag-Wolf, and B. Bewig. 2008. Standardized quantification of pulmonary fibrosis in histological samples. *Biotechniques* 44: 507-511, 514-507.
27. Gasse, P., N. Riteau, R. Vacher, M. L. Michel, A. Fautrel, F. di Padova, L. Fick, S. Charron, V. Lagente, G. Eberl, M. Le Bert, V. F. Quesniaux, F. Huaux, M. Leite-de-Moraes, B. Ryffel, and I. Couillin. 2011. IL-1 and IL-23 mediate early IL-17A production in pulmonary inflammation leading to late fibrosis. *PloS one* 6: e23185.
28. Zhao, Q., M. Manohar, Y. Wei, S. J. Pandol, and A. Habtezion. 2019. STING signalling protects against chronic pancreatitis by modulating Th17 response. *Gut*.
29. Ishikawa, H., and G. N. Barber. 2008. STING is an endoplasmic reticulum adaptor that facilitates innate immune signalling. *Nature* 455: 674-678.
30. Iurescia, S., D. Fioretti, and M. Rinaldi. 2018. Targeting Cytosolic Nucleic Acid-Sensing Pathways for Cancer Immunotherapies. *Front Immunol* 9: 711.
31. Wu, J. J., L. Zhao, H. G. Hu, W. H. Li, and Y. M. Li. 2019. Agonists and inhibitors of the STING pathway: Potential agents for immunotherapy. *Medicinal research reviews*.
32. Paludan, S. R., and A. G. Bowie. 2013. Immune sensing of DNA. *Immunity* 38: 870-880.
33. Pelka, K., T. Shibata, K. Miyake, and E. Latz. 2016. Nucleic acid-sensing TLRs and autoimmunity: novel insights from structural and cell biology. *Immunol Rev* 269: 60-75.
34. Falahat, R., P. Perez-Villarroel, A. W. Mailloux, G. Zhu, S. Pilon-Thomas, G. N. Barber, and J. J. Mulé. 2019. STING Signaling in Melanoma Cells Shapes Antigenicity and Can Promote Antitumor T-cell Activity. *Cancer immunology research* 7: 1837-1848.
35. Yi, G., V. P. Brendel, C. Shu, P. Li, S. Palanathan, and C. Cheng Kao. 2013. Single nucleotide polymorphisms of human STING can affect innate immune response to cyclic dinucleotides. *PloS one* 8: e77846.
36. Liu, Y., A. A. Jesus, B. Marrero, D. Yang, S. E. Ramsey, G. A. M. Sanchez, K. Tenbrock, H. Wittkowski, O. Y. Jones, H. S. Kuehn, C. R. Lee, M. A. DiMattia, E. W. Cowen, B. Gonzalez, I. Palmer, J. J. DiGiovanna, A. Biancotto, H. Kim, W. L. Tsai, A. M. Trier, Y. Huang, D. L. Stone, S. Hill, H. J. Kim, C. St Hilaire, S. Gurprasad, N. Plass, D. Chapelle, I. Horkayne-Szakaly, D. Foell, A. Barysenka, F. Candotti, S. M. Holland, J. D. Hughes, H. Mehmet, A. C. Issekutz, M. Raffeld, J. McElwee, J. R. Fontana, C. P. Minniti, S. Moir, D. L. Kastner, M. Gadina, A. C. Steven, P. T. Wingfield, S. R. Brooks, S. D. Rosenzweig,

T. A. Fleisher, Z. Deng, M. Boehm, A. S. Paller, and R. Goldbach-Mansky. 2014. Activated STING in a vascular and pulmonary syndrome. *N Engl J Med* 371: 507-518.
37. Jeremiah, N., B. Neven, M. Gentili, I. Callebaut, S. Maschalidi, M. C. Stolzenberg, N. Goudin, M. L. Fremond, P. Nitschke, T. J. Molina, S. Blanche, C. Picard, G. I. Rice, Y. J. Crow, N. Manel, A. Fischer, B. Bader-Meunier, and F. Rieux-Laucat. 2014. Inherited STING-activating mutation underlies a familial inflammatory syndrome with lupus-like manifestations. *J Clin Invest* 124: 5516-5520.
38. Clarke, S. L., E. J. Pellowe, A. A. de Jesus, R. Goldbach-Mansky, T. N. Hilliard, and A. V. Ramanan. 2016. Interstitial Lung Disease Caused by STING-associated Vasculopathy with Onset in Infancy. *American journal of respiratory and critical care medicine* 194: 639-642.
39. Bouis, D., P. Kirstetter, F. Arbogast, D. Lamon, V. Delgado, S. Jung, C. Ebel, H. Jacobs, A. M. Knapp, N. Jeremiah, A. Belot, T. Martin, Y. J. Crow, I. André-Schmutz, A. S. Korganow, F. Rieux-Laucat, and P. Soulas-Sprauel. 2019. Severe combined immunodeficiency in stimulator of interferon genes (STING) V154M/wild-type mice. *J Allergy Clin Immunol* 143: 712-725.e715.
40. Wu, J., and Z. J. Chen. 2014. Innate immune sensing and signaling of cytosolic nucleic acids. *Annu Rev Immunol* 32: 461-488.
41. Porat, A., E. Giat, C. Kowal, M. He, M. Son, E. Latz, I. Ben-Zvi, Y. Al-Abed, and B. Diamond. 2018. DNA-Mediated Interferon Signature Induction by SLE Serum Occurs in Monocytes Through Two Pathways: A Mechanism to Inhibit Both Pathways. *Front Immunol* 9: 2824.
42. Chamilos, G., J. Gregorio, S. Meller, R. Lande, D. P. Kontoyiannis, R. L. Modlin, and M. Gilliet. 2012. Cytosolic sensing of extracellular self-DNA transported into monocytes by the antimicrobial peptide LL37. *Blood* 120: 3699-3707.
43. Poli, C., J. F. Augusto, J. Dauve, C. Adam, L. Preisser, V. Larochette, P. Pignon, A. Savina, S. Blanchard, J. F. Subra, A. Chevailler, V. Procaccio, A. Croue, C. Creminon, A. Morel, Y. Delneste, H. Fickenscher, and P. Jeannin. 2017. IL-26 Confers Proinflammatory Properties to Extracellular DNA. *J Immunol* 198: 3650-3661.
44. Ryu, C., H. Sun, M. Gulati, J. D. Herazo-Maya, Y. Chen, A. Osafo-Addo, C. Brandsdorfer, J. Winkler, C. Blaul, J. Faunce, H. Pan, T. Woolard, A. Tzouvelekis, D. E. Antin-Ozerkis, J. T. Puchalski, M. Slade, A. L. Gonzalez, D. F. Bogenhagen, V. Kirillov, C. Feghali-Bostwick, K. Gibson, K. Lindell, R. I. Herzog, C. S. Dela Cruz, W. Mehal, N. Kaminski, E. L. Herzog, and G. Trujillo. 2017. Extracellular Mitochondrial DNA Is Generated by Fibroblasts and Predicts Death in Idiopathic Pulmonary Fibrosis. *American journal of respiratory and critical care medicine* 196: 1571-1581.
45. Qiu, H., D. Weng, T. Chen, L. Shen, S. S. Chen, Y. R. Wei, Q. Wu, M. M. Zhao, Q. H. Li, Y. Hu, Y. Zhang, Y. Zhou, Y. L. Su, F. Zhang, L. Q. Lu, N. Y. Zhou, S. L. Li, L. L. Zhang, C. Wang, and H. P. Li. 2017. Stimulator of Interferon Genes Deficiency in Acute Exacerbation of Idiopathic Pulmonary Fibrosis. *Front Immunol* 8: 1756.
46. Lemos, H., L. Huang, P. R. Chandler, E. Mohamed, G. R. Souza, L. Li, G. Pacholczyk, G. N. Barber, Y. Hayakawa, D. H. Munn, and A. L. Mellor. 2014. Activation of the STING adaptor attenuates experimental autoimmune encephalitis. *J Immunol* 192: 5571-5578.
47. Benmerzoug, S., S. Rose, B. Bounab, D. Gosset, L. Duneau, P. Chenuet, L. Mollet, M. Le Bert, C. Lambers, S. Geleff, M. Roth, L. Fauconnier, D. Sedda, C. Carvalho, O. Perche, D. Laurenceau, B. Ryffel, L. Apetoh, A. Kiziltunc, H. Uslu, F. S. Albez, M. Akgun, D. Togbe, and V. F. J. Quesniaux. 2018. STING-dependent sensing of self-DNA drives silica-induced lung inflammation. *Nat Commun* 9: 5226.
48. Iracheta-Vellve, A., J. Petrasek, B. Gyongyosi, A. Satishchandran, P. Lowe, K. Kodys, D. Catalano, C. D. Calenda, E. A. Kurt-Jones, K. A. Fitzgerald, and G. Szabo. 2016.

Endoplasmic Reticulum Stress-induced Hepatocellular Death Pathways Mediate Liver Injury and Fibrosis via Stimulator of Interferon Genes. *J Biol Chem* 291: 26794-26805.

49. Luksch, H., W. A. Stinson, D. J. Platt, W. Qian, G. Kalugotla, C. A. Miner, B. G. Bennion, A. Gerbaulet, A. Rosen-Wolff, and J. J. Miner. 2019. STING-associated lung disease in mice relies on T cells but not type I interferon. *J Allergy Clin Immunol*.
50. Warner, J. D., R. A. Irizarry-Caro, B. G. Bennion, T. L. Ai, A. M. Smith, C. A. Miner, T. Sakai, V. K. Gonugunta, J. Wu, D. J. Platt, N. Yan, and J. J. Miner. 2017. STING-associated vasculopathy develops independently of IRF3 in mice. *J Exp Med* 214: 3279-3292.
51. Gul, E., E. H. Sayar, B. Gungor, F. K. Eroglu, N. Surucu, S. Keles, S. N. Guner, S. Findik, E. Alpdundar, I. C. Ayanoglu, B. Kayaoglu, B. N. Geckin, H. A. Sanli, T. Kahraman, C. Yakicier, M. Muftuoglu, B. Oguz, D. N. Cagdas Ayvaz, I. Gursel, S. Ozen, I. Reisli, and M. Gursel. 2018. Type I IFN-related NETosis in ataxia telangiectasia and Artemis deficiency. *J Allergy Clin Immunol* 142: 246-257.
52. Blazek, K., H. L. Eames, M. Weiss, A. J. Byrne, D. Perocheau, J. E. Pease, S. Doyle, F. McCann, R. O. Williams, and I. A. Udalova. 2015. IFN-lambda resolves inflammation via suppression of neutrophil infiltration and IL-1beta production. *J Exp Med* 212: 845-853.
53. Broggi, A., Y. Tan, F. Granucci, and I. Zanoni. 2017. IFN-lambda suppresses intestinal inflammation by non-translational regulation of neutrophil function. *Nat Immunol* 18: 1084-1093.
54. Lee, K. G., S. S. Kim, L. Kui, D. C. Voon, M. Mauduit, P. Bist, X. Bi, N. A. Pereira, C. Liu, B. Sukumaran, L. Renia, Y. Ito, and K. P. Lam. Bruton's tyrosine kinase phosphorylates DDX41 and activates its binding of dsDNA and STING to initiate type 1 interferon response. *Cell Rep* 10: 1055-1065.
55. Parvatiyar, K., Z. Zhang, R. M. Teles, S. Ouyang, Y. Jiang, S. S. Iyer, S. A. Zaver, M. Schenk, S. Zeng, W. Zhong, Z. J. Liu, R. L. Modlin, Y. J. Liu, and G. Cheng. The helicase DDX41 recognizes the bacterial secondary messengers cyclic di-GMP and cyclic di-AMP to activate a type I interferon immune response. *Nat Immunol* 13: 1155-1161.
56. Dunphy, G., S. M. Flannery, J. F. Almine, D. J. Connolly, C. Paulus, K. L. Jønsson, M. R. Jakobsen, M. M. Nevels, A. G. Bowie, and L. Unterholzner. 2018. Non-canonical Activation of the DNA Sensing Adaptor STING by ATM and IFI16 Mediates NF-κB Signaling after Nuclear DNA Damage. *Molecular cell* 71: 745-760.e745.
57. Lei, Z., M. Deng, Z. Yi, Q. Sun, R. A. Shapiro, H. Xu, T. Li, P. A. Loughran, J. E. Griepentrog, H. Huang, M. J. Scott, F. Huang, and T. R. Billiar. 2018. cGAS-mediated autophagy protects the liver from ischemia-reperfusion injury independently of STING. *American journal of physiology. Gastrointestinal and liver physiology* 314: G655-g667.
58. Kinder, B. W., K. K. Brown, M. I. Schwarz, J. H. Ix, A. Kervitsky, and T. E. King, Jr. 2008. Baseline BAL neutrophilia predicts early mortality in idiopathic pulmonary fibrosis. *Chest* 133: 226-232.
59. Xaubet, A., C. Agusti, P. Luburich, J. A. Barbera, M. Carrion, M. C. Ayuso, J. Roca, and R. Rodriguez-Roisin. 1998. Interleukin-8 expression in bronchoalveolar lavage cells in the evaluation of alveolitis in idiopathic pulmonary fibrosis. *Respiratory medicine* 92: 338-344.
60. Gieseck, R. L., 3rd, M. S. Wilson, and T. A. Wynn. 2018. Type 2 immunity in tissue repair and fibrosis. *Nat Rev Immunol* 18: 62-76.
61. Wynn, T. A., and K. M. Vannella. 2016. Macrophages in Tissue Repair, Regeneration, and Fibrosis. *Immunity* 44: 450-462.
62. Kitowska, K., D. Zakrzewicz, M. Königshoff, I. Chrobak, F. Grimminger, W. Seeger, P. Bulau, and O. Eickelberg. 2008. Functional role and species-specific contribution of arginases in pulmonary fibrosis. *Am J Physiol Lung Cell Mol Physiol* 294: L34-45.

63. Vono, M., A. Lin, A. Norrby-Teglund, R. A. Koup, F. Liang, and K. Loré. 2017. Neutrophils acquire the capacity for antigen presentation to memory CD4(+) T cells in vitro and ex vivo. *Blood* 129: 1991-2001.
64. Li, Y., W. Wang, F. Yang, Y. Xu, C. Feng, and Y. Zhao. 2019. The regulatory roles of neutrophils in adaptive immunity. *Cell communication and signaling : CCS* 17: 147.

Figure Legends

Figure 1. Increased BALF dsDNA content as well as cGAS and STING expressions

C57BL/6 WT, *Cgas*$^{-/-}$ and *Sting*$^{-/-}$ mice were treated with NaCl or BLM (3mg/kg intranasally) and BALF and lungs were collected after 14 days. **(A)** BALF cell-free dsDNA content. **(B)** *Mb21d1* (cGAS) and **(C)** *Tmem173* (STING) gene expressions. STING protein expression by **(D)** Western-Blotting and **(E)** semi-quantitative band analysis. **(F)** STING expression in the lungs assessed by immunofluorescence. The yellow box is magnified in **(G)** and yellow arrows illustrate STING positive infiltrating cells. Data are representative of 2-3 independent experiments, showed as mean ± SEM, *:$p<0.05$; ***:$p<0.001$.

Figure 2. Increased fibrosis in absence of STING

WT, *Cgas*$^{-/-}$ and *Sting*$^{-/-}$ mice were treated with NaCl or BLM (3mg/kg intranasally) and BALF and lungs were collected after 14 days. **(A)** Body weight evolution. Asterisks depict $p<0.05$ comparing BLM-treated WT and *Sting*$^{-/-}$ groups at indicated time points **(B)** MMP-9 and **(C)** TIMP-1 levels in the lungs measured by ELISA. **(D)** Lung micrographs stained by Hematoxylin and Eosin (H&E). **(E)** $CD4^+$ T lymphocyte numbers in the lung left lobe. **(F)** Lung micrographs

582 stained by Red Sirius/Fast Green highlighting collagen fibers. **(G)** Fibrosis score using Ashcroft
583 modified scale. **(H)** BALF collagen content measured by Sircol assay. **(I)** TGF-β1-3 in the lungs
584 measured by multiplex assay. Data are representative of 2-3 independent experiments, showed as
585 mean ± SEM, ns: non-significant; *:p<0.05; **:p<0.01; ***:p<0.001.

586

587 **Figure 3. STING deficiency leads to increased fibrosis independently of type I IFN signaling**
588 WT, *Sting*$^{-/-}$ and type I Interferon receptor deficient (*Ifnar1*$^{-/-}$) mice were treated with NaCl or BLM
589 (3mg/kg intranasally) and BALF and lungs were collected after 14 days. **(A)** Body weight
590 evolution. Asterisks depict p<0.05 comparing BLM-treated WT and *Sting*$^{-/-}$ groups at indicated
591 time points. **(B)** MMP-9 and **(C)** TIMP-1 levels in the lungs measured by ELISA. Lung
592 micrographs stained by **(D)** Hematoxylin and Eosin (H&E) (black arrows show cell foci) and **(E)**
593 Red Sirius/Fast Green highlighting collagen fibers. Higher magnification are depicted using red
594 and blue rectangles and black arrows show collagen deposition. **(F)** Fibrosis score using Ashcroft
595 modified scale. **(G)** Lung *fibronectin 1* gene expression by RT qPCR. **(H)** Frequencies and **(I)** total
596 numbers of lung $CD4^+$ $IL\text{-}17^+$ T cells assessed by flow cytometry. Data are representative of 2-3
597 independent experiments, showed as mean ± SEM, ns: non-significant *:p<0.05; **:p<0.01;
598 ***:p<0.001.

599

600 **Figure 4. STING deficiency leads to dysregulated neutrophils.**

601 WT, *Cgas*$^{-/-}$ and *Sting*$^{-/-}$ mice were treated with NaCl or BLM (3mg/kg intranasally) and BALF
602 and lungs were collected after 14 days. (**A**) Flow cytometry gating strategy used to identify **(B)**

BALF cell populations. Cells are gated on singlets, live, $CD45^+$ events. NP: Neutrophils; AM: Alveolar macrophages. Total BALF cell numbers **(C)**, neutrophil **(D)** BALF total numbers and **(E)** lung percentages. **(F)** Kinetic of BALF neutrophil frequencies at indicated time points. MHC-II **(G-H)** and Arginase-1 **(I-J)** Mean Fluorescence Intensity (MFI) assessed by flow cytometry. Data are representative of 2-3 independent experiments, showed as mean ± SEM, *:p<0.05; ***:p<0.001.

Supplementary Figure 1. WT, *Cgas*$^{-/-}$ and *Sting*$^{-/-}$ mice were treated with NaCl or BLM (7mg/kg intranasally) and BALF and lungs were collected at 24 hours. **(A)** BALF cell-free dsDNA content. BALF **(B)** total numbers and **(C)** neutrophil frequencies. KC/CXCL-1 **(D)**, MMP-9 **(E)** and TIMP-1 **(F)** levels in the lungs measured by ELISA. Data are a pool of 2-3 independent experiments showed as mean ± SEM, ns: non-significant; ***:p<0.001.

Supplementary Figure 2. WT, *Sting*$^{-/-}$ and *Ifnar1*$^{-/-}$ mice were treated with NaCl or BLM (3mg/kg intranasally) and lungs cells were collected after 14 days and incubated for 5 hours at 37°C in presence of BFA . **(A)** Gating strategy employed to delineate lung IL-$17A^+$ $CD4^+$ T lymphocytes. **(B)** Representative flow cytometry plots. Data are representative of 2 independent experiments.

Supplementary Figure 3. WT, *Cgas*$^{-/-}$, *Sting*$^{-/-}$ and *Ifnar1*$^{-/-}$ mice were treated with NaCl or BLM (3mg/kg intranasally) and lungs were collected after 14 days. (**A**) IL-28 content in the lungs measured by ELISA and **(B)** by Western-Blotting with **(C)** semi-quantitative band analysis. Data

are representative of 2 independent experiments showed as mean ± SEM, ns: non-significant; *:$p<0.05$

Supplementary Figure 4. Gating strategy used to delineate neutrophil populations **(A)** in the BALF and **(B)** in the lungs by flow cytometry.

Figure 1

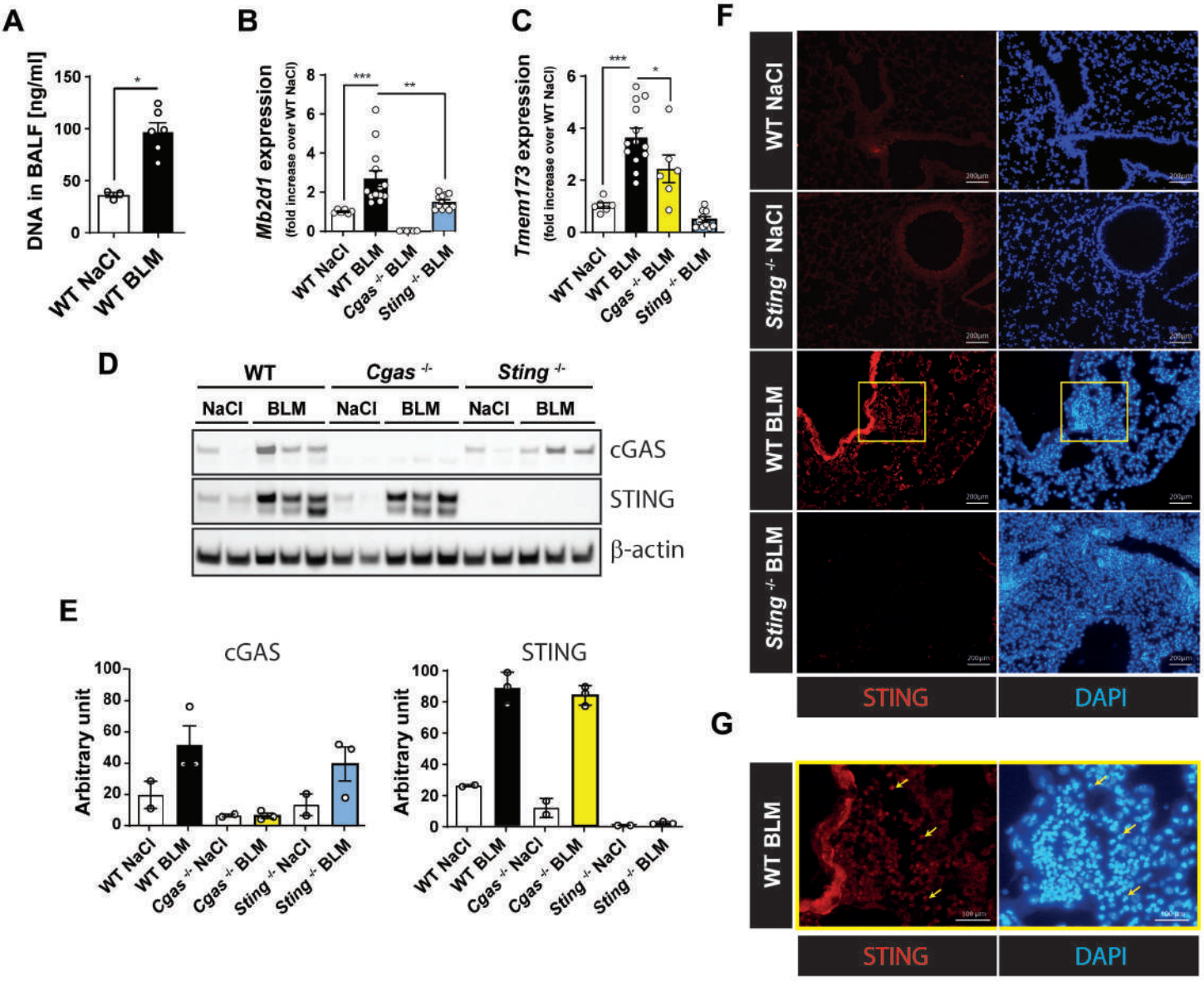
A
DNA in BALF [ng/ml]
150
100
50
0
*
WT NaCl
WT BLM
B
Mb2d1 expression
(fold increase over WT NaCl)
8
6
4
2
0
***
**
WT NaCl
WT BLM
Cgas -/- BLM
Sting -/- BLM
C
Tmem173 expression
(fold increase over WT NaCl)
6
4
2
0
***
*
WT NaCl
WT BLM
Cgas -/- BLM
Sting -/- BLM
D
WT
Cgas -/-
Sting -/-
NaCl
BLM
NaCl
BLM
NaCl
BLM
cGAS
STING
β-actin
E
cGAS
STING
Arbitrary unit
100
80
60
40
20
0
WT NaCl
WT BLM
Cgas -/- NaCl
Cgas -/- BLM
Sting -/- NaCl
Sting -/- BLM
F
WT NaCl
Sting -/- NaCl
WT BLM
Sting -/- BLM
STING
DAPI
G
WT BLM
STING
DAPI

Figure 2

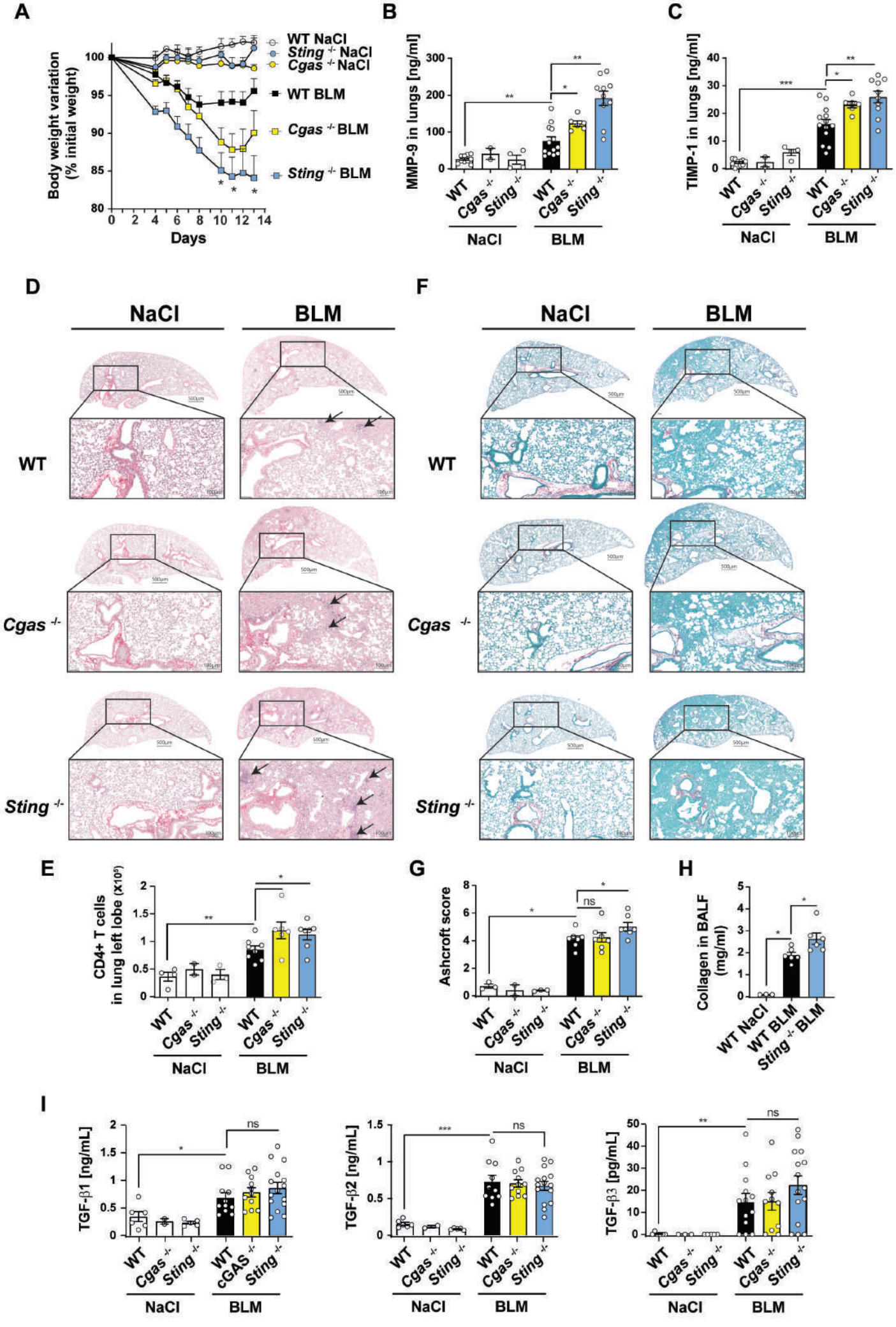
A
Body weight variation (% initial weight)
Days
WT NaCl
Sting -/- NaCl
Cgas -/- NaCl
WT BLM
Cgas -/- BLM
Sting -/- BLM
B
MMP-9 in lungs [ng/ml]
C
TIMP-1 in lungs [ng/ml]
WT
Cgas -/-
Sting -/-
NaCl
BLM
D
F
NaCl
BLM
WT
Cgas -/-
Sting -/-
E
CD4+ T cells in lung left lobe (X10⁵)
G
Ashcroft score
H
Collagen in BALF (mg/ml)
WT NaCl
WT BLM
Sting -/- BLM
I
TGF-β1 [ng/mL]
TGF-β2 [ng/mL]
TGF-β3 [pg/mL]
cGAS -/-
ns

Figure 3

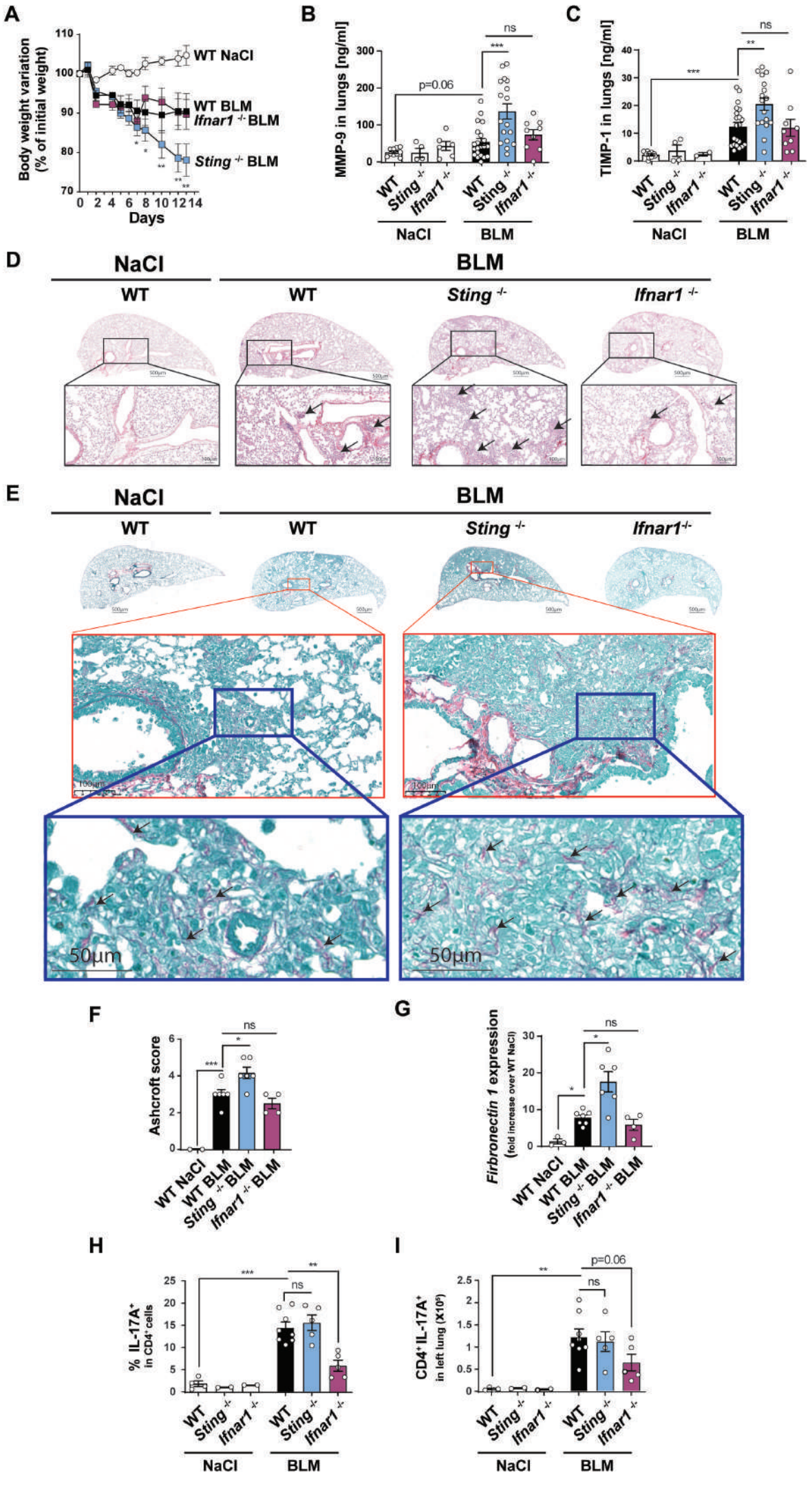
A
Body weight variation (% of initial weight)
Days
WT NaCl
WT BLM
Ifnar1 -/- BLM
Sting -/- BLM
B
MMP-9 in lungs [ng/ml]
p=0.06
ns
NaCl
BLM
C
TIMP-1 in lungs [ng/ml]
D
NaCl
BLM
WT
Sting -/-
Ifnar1 -/-
E
50µm
F
Ashcroft score
G
Firbronectin 1 expression
(fold increase over WT NaCl)
H
% IL-17A+ in CD4+ cells
I
CD4+IL-17A+ in left lung (X10⁶)

Figure 4

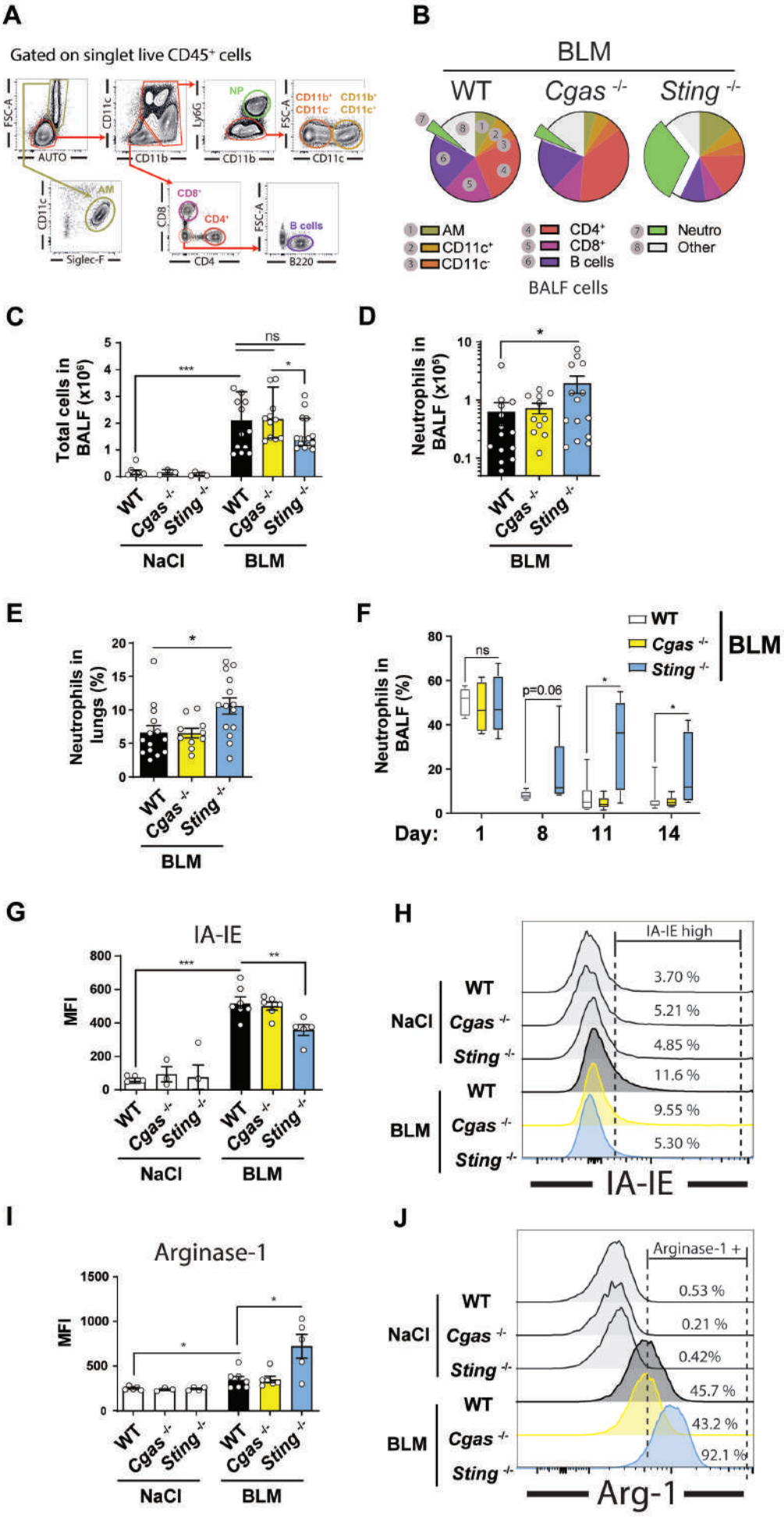
A
Gated on singlet live CD45+ cells
FSC-A
AUTO
CD11c
CD11b
Ly6G
NP
CD11b+ CD11c+
CD11b+ CD11c-
CD11c
AM
Siglec-F
CD8
CD8+
CD4+
CD4
FSC-A
B cells
B220
B
BLM
WT
Cgas -/-
Sting -/-
1 AM
2 CD11c+
3 CD11c-
4 CD4+
5 CD8+
6 B cells
7 Neutro
8 Other
BALF cells
C
Total cells in BALF (x10^6)
ns
***
*
WT
Cgas -/-
Sting -/-
NaCl
BLM
D
Neutrophils in BALF (x10^5)
*
BLM
E
Neutrophils in lungs (%)
*
BLM
F
Neutrophils in BALF (%)
WT
Cgas -/-
Sting -/-
BLM
ns
p=0.06
*
*
Day: 1 8 11 14
G
IA-IE
MFI
***
**
NaCl
BLM
H
IA-IE high
NaCl
BLM
WT
Cgas -/-
Sting -/-
3.70 %
5.21 %
4.85 %
11.6 %
9.55 %
5.30 %
IA-IE
I
Arginase-1
MFI
*
*
NaCl
BLM
J
Arginase-1 +
NaCl
BLM
0.53 %
0.21 %
0.42%
45.7 %
43.2 %
92.1 %
Arg-1

Supplementary Figure 1

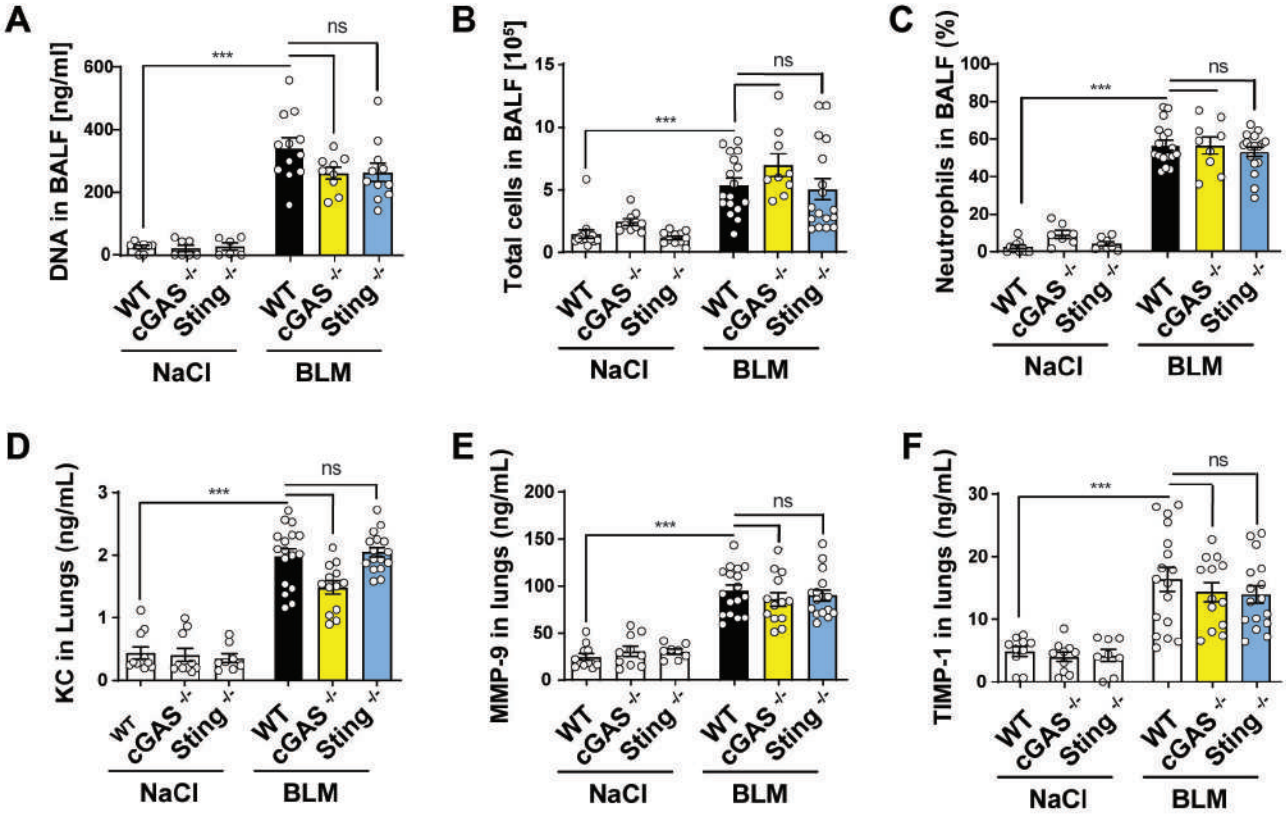

Supplementary Figure 2

A Gating strategy for IL-17 producing lung CD4⁺ T lymphocytes

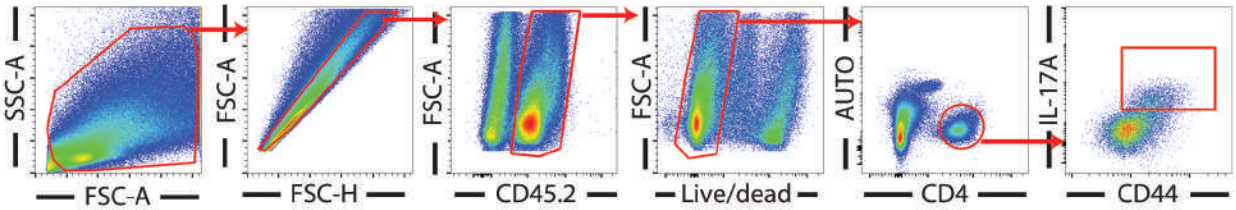

B

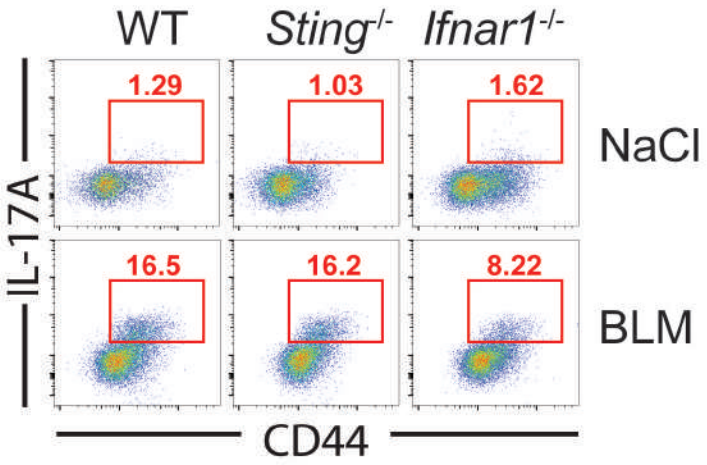

Supplementary Figure 3

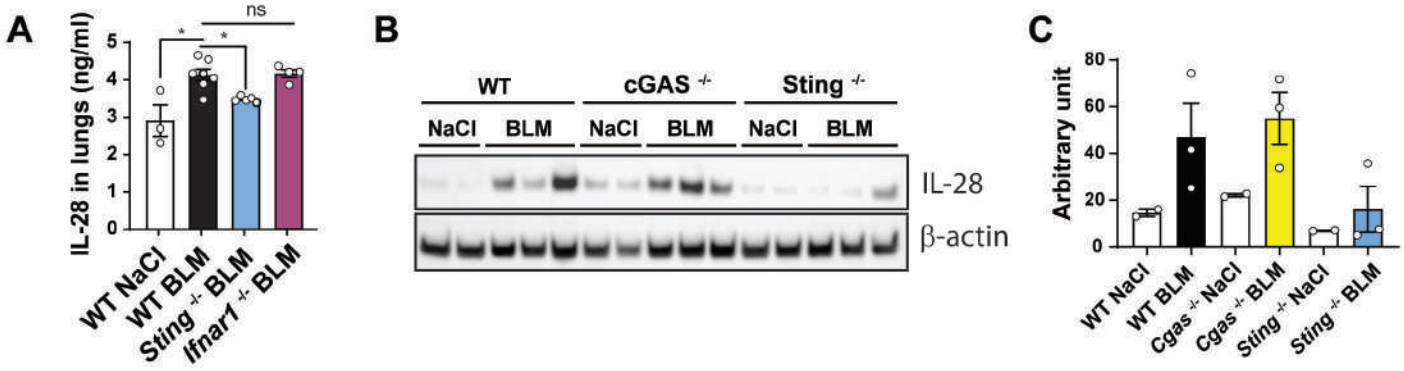

Supplementary Figure 4

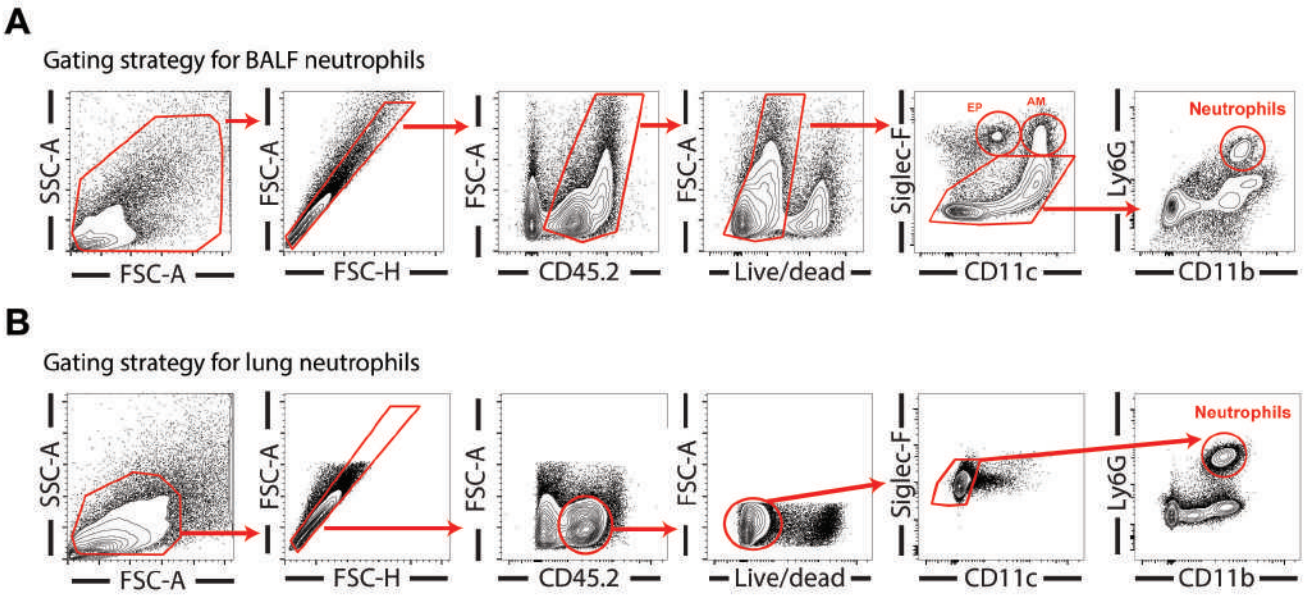

Supplementary Table 1

Antibody	Clone	Application	Dilution
Arginase 1	A1exF5	FC	1/100
B220	RA3-6B2	FC	1/200
CD11b	M1/70	FC	1/300
CD11c	N418	FC	1/200
CD4	RM4-5	FC	1/200
CD44	IM7	FC	1/200
CD45.2	104	FC	1/200
CD8a	53-6.7	FC	1/200
CD8b	H35-17.2	FC	1/200
F4/80	BM8	FC	1/300
IA-IE	M5/114.15.2	FC	1/400
IL-17A	eBio17B7	FC	1/100
Live/Dead		FC	1/800
Siglec-F	E50-2440	FC	1/300
Sting	polyclonal	IF	1/1000
β-actin	clone AC-15	WB	1/20000
Cgas	"D3O8O"	WB	1/1000
IL-28	D-12	WB	1/500
Sting	polyclonal	WB	1/1000

Supplementary Table 1: List of applications, clones and dilutions of the antidodies used. FC: Flow cytometry, IF: Immunofluorescence, WB: Western-Blot